Inorganic Chemistry
Article

Inorg. Chem. **2010**, *49*, 10949–10955 **10949**
DOI: 10.1021/ic101324e

Formation of Nanometric HT-$LiCoO_2$ by a Precipitation and Aging Process in an Alcoholic Solution

Dominique Larcher,[†,‡] Bruno Delobel,[†,‡] Lydia Dantras-Laffont,[†] Evelyne Simon,[§] Jean-François Blach,[⊥] and Emmanuel Baudrin*[,†,‡]

[†]*Laboratoire de Réactivité et Chimie des Solides, UMR CNRS 6007, Université de Picardie Jules Verne, 33 rue Saint Leu, 80039 Amiens Cedex, France,* [§]*European Space Agency, ESTEC, Keplerlaan 1, 2200AG Noordwijk, The Netherlands,* [⊥]*Faculté des Sciences Jean Perrin, Rue Jean Souvraz, Unité de Catalyse et de Chimie du Solide, UCCS, CNRS-UMR 8181, Université Lille Nord de France (UA), SP 18, 62307 Lens Cedex, France, and* [‡]*ALISTORE-ERI European Research Institute, FR CNRS No. 3104, 33 rue Saint Leu, 80039 Amiens Cedex, France*

Received July 2, 2010

In this paper, we detailed the formation/evolution of precipitates in alcoholic media containing Co^{II+} and Li^{+} species, together with the evolution of the composition and structure/texture of the resulting solid phases during the aging process at controlled constant temperature. While the end product is found to be well-crystallized HT-$LiCoO_2$, its formation is shown to result from a two-step process enlisting the initial fast precipitation of β-$HCoO_2$ and then its slow dissolution followed by recrystallization of the lithium-containing material. These results were obtained through combined X-ray diffraction, Raman and IR spectroscopy, elemental and oxidation-state analysis, and high-resolution transmission electron microscopy/selected-area electron diffraction observations. Depending on the cationic concentration, the size of the precipitated material can be controlled within the nanometric range. The electrochemical performances of these aged materials are slightly improved compared to those of the directly precipitated ones that we previously reported. The main limitation of these materials remains the presence of surface protons.

Introduction

Since the first commercialization of Li-ion batteries by Sony in 1991.[1] This technology has progressively captured the energy storage market for mobile applications such as laptops and cell phones. Today, it is considered to be the most suited technology for near-future electric (EVs) and hybrid electric (HEVs) vehicles. The success of this technology is mainly nested in high specific energy density and cycle life/efficiency compared to other energy storage devices.[2] To further improve their performances, a huge amount of work has been pursued mainly focused on electrode materials and electrolyte formulation, thus leading to constant but still slow incremental improvements during the 1980s and 1990s. Recently, the study of new classes of materials and the demonstration of new Li-ion reactivities considerably widened the spectrum of possibilities and concomitantly prompted investigations toward nanomaterials. This evolution was rapidly implemented in commercial systems, thus boosting their performances.

As a consequence, the controlled preparation of highly divided electrode materials and the understanding of the related "nanoscale" mechanisms are crucial. The present paper is a contribution to this.

Despite the toxicity of cobalt and the competition with other emerging materials such as $LiFePO_4$, $LiCoO_2$ and related substituted materials are still among the most used positive-electrode materials for Li-ion batteries. Since the demonstration by Goodenough's group in the early 1980s[3] of the excellent electrochemical properties of HT-$LiCoO_2$ (the high-temperature polymorph), the enormous knowledge gathered on its properties and preparation routes makes this phase a "model system" to scrutinize alternative preparation processes and their impact on electrochemical reactivity.

The preparation of this layered (space group $R\bar{3}m$), high-temperature polymorph (HT-$LiCoO_2$) generally requires annealing treatments at temperatures higher than 800 °C to ensure a satisfactory Li/Co ordering.[4] The synthesis method/parameters can dramatically alter this ordering and, consequently, impair the related electrochemical performances.

*To whom correspondence should be addressed. E-mail: emmanuel.baudrin@u-picardie.fr. Tel.: +33-322827493. Fax: +33-322827469.

(1) Sony Lithium Ion Battery Performance Summary. *JEC Batt.* **1994**, *2*, 31.
(2) Tarascon, J.-M.; Armand, M. *Nature* **2001**, *414*, 359.
(3) Mizushima, K.; Jones, P. C.; Wiseman, P. J.; Goodenough, J. B. *Mater. Res. Bull.* **1980**, *15*, 783.
(4) Johnston, W. D.; Heikes, R. R.; Sestrich, D. *J. Phys. Chem. Solids* **1958**, *7*, 1.

Published on Web 10/29/2010

In this system, this is well exemplified by the low-temperature polymorph (LT-$LiCoO_2$), which adopts a spinel-type structure (space group $Fd\bar{3}m$), with 6% of Co atoms lying within the lithium layers.[5,6] Such mixing hinders the electrochemical performances with, namely, a relatively large polarization (300 mV) compared to the layered HT-$LiCoO_2$ (50 mV)[7] and a smaller energy density due to a lower lithium extraction voltage (3.65 V for LT-$LiCoO_2$ and 3.9 V for HT-$LiCoO_2$ vs Li^+/Li^0).

Although HT-$LiCoO_2$ has excellent electrochemical characteristics,[1,3] the use of micrometer-sized powders leads to limitations for high-power applications such as electrical vehicles or peculiar space applications. Among other ways, this can be alleviated by downsizing the particle toward the nanometric range, thus compensating for the electronic and ionic transport limitations, as exemplified by $LiFePO_4$[8] or titanates.[9] In the Li−Co−O system, the preparation of nanoscale particles with the lamellar structure is not trivial because the nanomaterials are usually formed by low-temperature processes, thus favoring the LT-$LiCoO_2$ phase.[10] However, some reports indicate that nanosized HT-$LiCoO_2$ can be produced under hydrothermal conditions,[11,12] through molten-salt reactions,[13] by coprecipitation,[14] or by spray-drying.[15] Among these routes, low-temperature precipitation reactions (i.e., inorganic polymerization) enable control of the size, texture, and composition of the precipitated powders[16,17] provided that the solvent is carefully selected. As a matter of fact, there is here a double challenge in preparing nanosized HT-$LiCoO_2$ through such "Chimie Douce" routes because of their tendency to favor the low-temperature polymorph (LT-$LiCoO_2$) and also because of the inability of water, used as solvent, to enable the simultaneous hydrolysis of lithium and cobalt species, mandatory for condensation of mixed lithium−cobalt oxides.

We recently reported the direct one-step precipitation of layered nanosized $LiCoO_2$ materials at room temperature in highly basic alcoholic media (methanol, ethanol, and propanol) as an alternative to aqueous media.[18] In that case, the reactions were performed without any aging step, the solids being recovered straightaway after precipitation. The nature of the precipitated phases [the presence of small amounts of Co_3O_4 and rock salt $Li_xCo_{1-x}O$ phases as byproducts was noticed] can be modulated by the cationic composition of the solution, while the alcohol chain length enables fine control of the size of the monolithic particles. However, we did not succeed in obtaining solids approaching the expected stoichiometry. Indeed, we found a direct correlation between the particle size and the Li/Co stoichiometry explained by the presence of surface protons, the amount of which increases as the particles get smaller. When using ethanol as solvent, we prepared phases with stoichiometry close to "$H_{0.14}Li_{0.86}CoO_2$".

To better understand and control the precipitation within the Li−Co−O system in such alcoholic media, we here embarked on a mechanistic study of phase evolution during the thermostatic aging process of suspensions in ethanol. We will particularly enlighten an original $HCoO_2 \rightarrow LiCoO_2$ dissolution−crystallization mechanism and will address the influence of the nature of the alcohol, of the temperature, and of the co-ion concentration.

Experimental Section

Sample Preparation. Typically, 100 mL of an ethanol solution containing 2 M $LiNO_3$ and 0.4 M $Co(NO_3)_2 \cdot 6H_2O$ was added dropwise under constant stirring into 150 mL of a 3 M KOH/ethanol solution maintained at 60 °C. Then, 10 mL samples of the suspension were successively withdrawn after different reaction times ranging from 1 min to 7 days; these samples will be referred to as "LC-*time*". On the basis of our previous findings,[18] the as-precipitated powders are a mixture of the expected cobalt-based oxide with KNO_3 and Li_2CO_3. These two impurities were subsequently eliminated by a washing step in LiOH aqueous solutions (500 mL, 10^{-1} M, 2 days), preventing $Li^+ \rightleftarrows H^+$ exchange. The resulting brown solids were separated from the supernatant by filtration through a 0.22 μm membrane, washed with acetone, and air-dried overnight at 80 °C.

The Co_3O_4 reference sample was synthesized by decomposition of $Co(NO_3)_2 \cdot 6H_2O$ at 800 °C under air for 10 h. A reference HT-$LiCoO_2$ batch was synthesized starting from a $LiNO_3$/$Co(NO_3)_2 \cdot 6H_2O$ ethanol solution (Li/Co = 1.05/1). After self-evaporation of the solvent and drying at 80 °C, the resulting solid was heated successively under air at 400 °C (1 °C·min^{-1}) for 5 h and at 850 °C for 12 h and then left to cool to ambient temperature inside the furnace.

For β-$HCoO_2$ synthesis, 100 mL of a 0.1 M $Co(NO_3)_2 \cdot 6H_2O$ aqueous solution was added dropwise into 200 mL of a 2 M NaOH aqueous solution. The resulting $Co(OH)_2$ suspension was aged for several days under stirring to enable the complete oxidation of Co^{II+} to Co^{III+} by atmospheric O_2. The powder was recovered by centrifugation, washed with distilled water, and finally dried at 50 °C overnight.

Powder Characterization. X-ray diffraction (XRD) patterns were collected at room temperature with a Bruker D8 diffractometer using Co Kα radiation (λ_1 = 1.78919 Å; λ_2 = 1.79321 Å) equipped with a position-sensitive detector. The refinement of the peak profile and cell-parameter refinements were carried out with *FullProf* software (Windows version, March 2007)[19] using the pseudo-Voigt profile function of Thompson, Cox, and Hastings.[20] In order to extract microstructural information from the peak profile, a corundum-type Al_2O_3 standard was

(5) Gummow, R. J.; Liles, D. C.; Thackeray, M. M. *Mater. Res. Bull.* **1992**, *27*(3), 327.
(6) Shao-Horn, Y.; Hackney, S. A.; Kahaian, A. J.; Thackeray, M. M. *J. Solid State Chem.* **2002**, *168*, 60.
(7) Gummow, R. J.; Liles, D. C.; Thackeray, M. M. *Mater. Res. Bull.* **1992**, *27*(3), 327.
(8) Delacourt, C.; Poizot, P.; Levasseur, S.; Masquelier, C. *Electrochem. Solid-State Lett.* **2006**, *9*, A352.
(9) Armstrong, A. R.; Armstrong, G.; Canales Garcia, J. R.; Bruce, P. G. *Adv. Mater.* **2005**, *17*, 862.
(10) Jiao, F.; Shaju, K. M.; Bruce, P. G. *Angew. Chem., Int. Ed.* **2005**, *44*, 6550.
(11) Larcher, D.; Palacin, M. R.; Amatucci, G. G.; Tarascon, J. M. *J. Electrochem. Soc.* **1997**, *144*, 408.
(12) Okubo, M.; Hosono, E.; Kim, J.; Enomoto, M.; Kojima, N.; Kudo, T.; Zhou, H.; Honma, I. *J. Am. Chem. Soc.* **2007**, *129*, 7444.
(13) Chen, H.; Grey, C. P. *Adv. Mater.* **2008**, *20*, 2206.
(14) Chen, H.; Qiu, X.; Zhu, W.; Hagenmuller, P. *Electrochem. Commun.* **2002**, *4*, 488.
(15) Li, Y.; Wan, C.; Wu, Y.; Jiang, C.; Zhu, Y. *J. Power Sources* **2000**, *85*, 294.
(16) Portehault, D.; Cassaignon, S.; Baudrin, E.; Jolivet, J.-P. *Chem. Mater.* **2007**, *19*, 5410.
(17) Binotto, G.; Larcher, D.; Prakash, A. S.; Herrera Urbina, R.; Hegde, M. S.; Tarascon, J.-M. *Chem. Mater.* **2007**, *19*, 3032.
(18) Delobel, B.; Larcher, D.; Blach, J.-F.; Croguennec, L.; Ménétrier, M.; Simon, E.; Baudrin, E. *Solid State Ionics* **2010**, *181*, 623.
(19) Rodríguez-Carvajal, J. *Physica B* **1992**, *192*, 55. For a more recent version, see: Rodríguez-Carvajal, J. *CPD Newsletter* **2001**, *26*, 12, available at http://journals.iucr.org/iucr-top/comm/cpd/Newsletters/. The program and documentation are available at http://www.ill.fr/dif/Soft/fp.
(20) Thompson, P.; Cox, D. E.; Hastings, J. B. *J. Appl. Crystallogr.* **1987**, *20*, 79.

used to determine the Instrumental Resolution Function (U = 0.018 336 deg^2, V = −0.012 039 deg^2, and W = 0.012 975 deg^2) of the instrument. Transmission electron microscopy (TEM) images were performed on a FEI Tecnai F20 S-TWIN microscope (200 kV), and the grids were prepared from a suspension of the powders in acetone and dispersed by ultrasonic treatment.

Raman spectra were recorded in backscattering geometry using a Dilor XY800 triple monochromator coupled with a microscope that focused the 514.5 nm laser beam to a 2 μm spot. A low-power laser beam (0.5 mW) was used to avoid possible changes due to local heating. The lithium and cobalt contents were estimated by atomic absorption spectroscopy (AAS; Perkin-Elmer AAnalyst 300). The cobalt mean oxidation state (mos) was determined by iodometric titration. The powder (20 mg) was dissolved in 20 mL of a 6 M HCl aqueous solution containing a large excess of potassium iodide (500 mg). I_2 resulting from the oxidation of iodide by Co^{III+} was back-titrated with a sodium thiosulfate solution (10^{-2} M) using starch as the end-reaction colorimetric indicator. The resulting solution was used to analyze the total cobalt content by AAS. It is important to underline that no noticeable matrix effect was detected in relation to the presence of starch-, iodine-, chlorine-, potassium-, or sulfur-based species.

Electrochemical measurements were carried out at 20 °C using a MacPile (Biologic SA, Claix, France) potentiostat in a galvanostatic mode at a rate of 1 Li every 10 h between 4.2 and 3.0 V vs Li^+/Li^0. The materials were ground with 20% by weight of Super P (TIMCAL) carbon for 5 min in a mortar. The electrochemical cells were made of about 10 mg of the latter mixture as the positive electrode and a lithium foil as the negative electrode with glass fiber disk separators soaked with 1 M $LiPF_6$ in EC/DMC (1:1, v/v) electrolyte. Throughout this paper, the cell potentials will always be given with respect to the Li^+/Li^0 couple.

Results and Discussion

The preparation method is based on a precipitation reaction in highly alkaline ethanol solutions using cobalt(II+) and lithium(+) nitrate precursors. When performed at ambient temperature, we previously observed that the Co ions oxidized by dissolved oxygen directly led to the Co^{III+}-containing HT-$LiCoO_2$ phase.[18] The mechanism is drastically different at 60 °C; the XRD patterns evidence the initial formation of β-$HCoO_2$ (LC-1 min) (Figure 1). This demonstrates a drastic influence of the temperature on the reaction mechanism. For reaction times beyond 1 h, the XRD patterns show the progressive growth of layered HT-$LiCoO_2$ at the expense of β-$HCoO_2$. Such an evolution is consistent with a biphasic transition because both phases are spotted simultaneously for LC-5 h and LC-10 h. From LC-1 d to LC-7 d, only $LiCoO_2$ is recovered without any visible trace of Co_3O_4 or rock salt Li−Co−O impurities.

The cell parameters for both phases were determined by the refinement of the whole set of XRD patterns using a full pattern matching procedure (Figure 2). From LC-1 min [a = 2.8518(1) Å and c = 13.154(2) Å] to LC-30 min, the cell parameters for the precipitated β-$HCoO_2$ match well those of our reference sample and the literature (a = 2.855 Å and c = 13.157 Å).[21] From LC-1 h to LC-10 h, pattern refinements confirm the presence of the two phases with some discrepancies from the references data that can be assigned to the fitting difficulty arising from the broadness of the peaks. For instance, in LC-10 h, a = 2.8217(2) Å and c = 14.114(3) Å

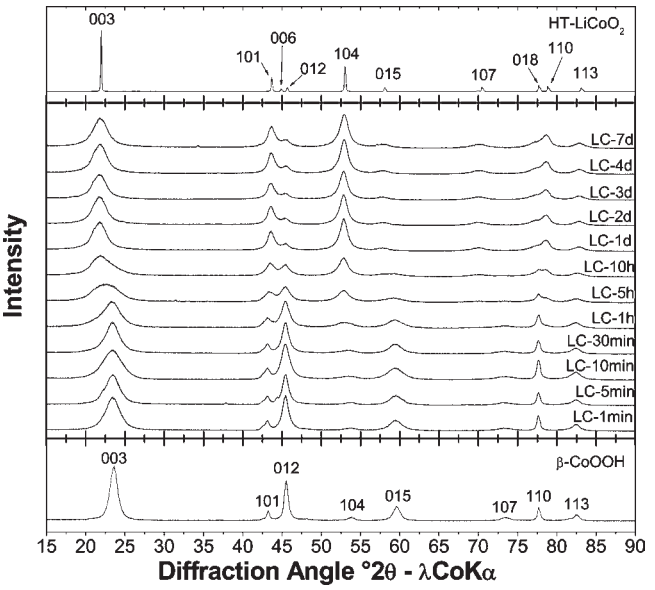

Figure 1. XRD patterns for precipitates recovered after 1 min (LC-1 min) to 7 days (LC-7 d) of aging at 60 °C of an ethanol solution containing $[Li^+]$ = 2 mol·L^{-1} and $[Co^{II+}]$ = 0.4 mol·L^{-1}. XRD patterns of HT-$LiCoO_2$ (top) and β-$HCoO_2$ (bottom) are shown as reference.

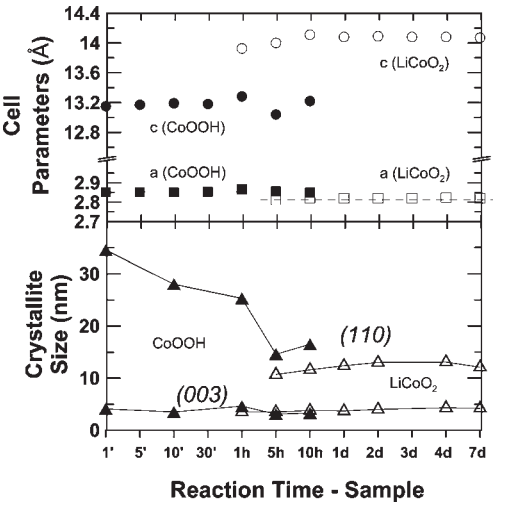

Figure 2. Evolution in the a and c cell parameters (top) and in the [003] and [110] crystallites size (bottom) for β-$HCoO_2$ and $LiCoO_2$ precipitated during aging of an ethanol solution with $[Li^+]$ = 2 mol·L^{-1} and $[Co^{II+}]$ = 0.4 mol·L^{-1} at 60 °C. Horizontal dashed lines indicate the cell-parameter values for β-$HCoO_2$ and $LiCoO_2$ as reference.

are refined for the $LiCoO_2$ phase to be compared to a = 2.8166 Å and c = 14.052 Å for reference.[4] After this biphasic domain, the $LiCoO_2$ cell-parameter values are stable, with, however, a noticeably larger c parameter than is usually reported (≈14.05 Å). Such a deviation has already been reported for nanometric $LiCoO_2$,[18] rutile TiO_2,[22] and $Ni(OH)_2$[23] and ascribed to surface relaxation due to a different coordination of the surface species, and thus amplified for nanometric materials compared to their bulk counterpart.

(21) Kondrashev, Y. D.; Fedorova, N. N. *Dokl. Akad. Nauk SSSR* **1954**, *94*, 229.

(22) Koelsch, M. Ph.D. Thesis, Université Pierre et Marie Curie: Paris, France, 2004.

(23) Casas-Cabanas, M.; Rodriguez-Carvajal, J.; Canales-Vasquez, J.; Palacin, M. R. *J. Mater. Chem.* **2006**, *16*, 2925.

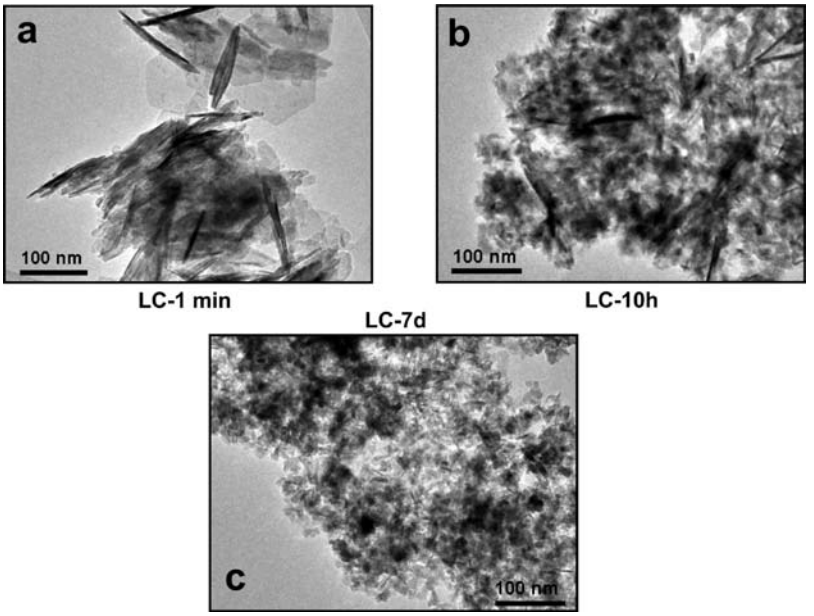

Figure 3. TEM pictures for LC-1 min (a), LC-10 h (b), and LC-7 d (c).

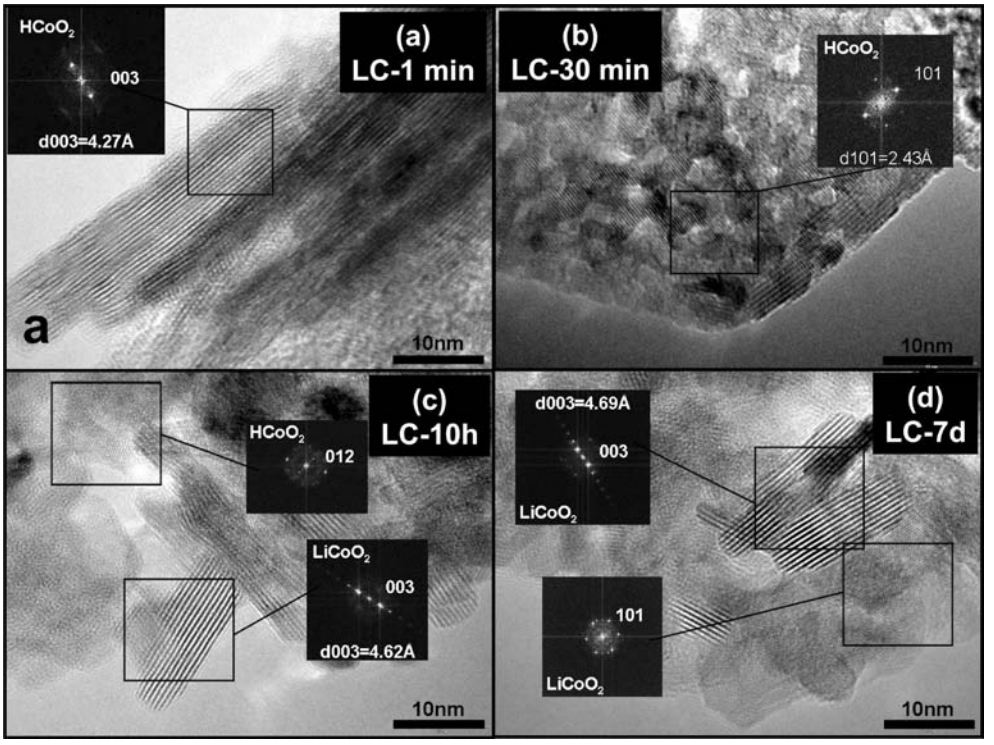

Figure 4. HR-TEM pictures for (a) LC-1 min, (b) LC-30 min, (c) LC-10 h, and (d) LC-7 d together with Fourier transformation of selected picture areas.

The crystallite size along the [003] direction (perpendicular to the CoO_2 layer), determined through refinement of the XRD patterns taking into account the microstructure,[19,20] is found to be almost constant during the whole aging process, ca. 4 nm (Figure 2). In contrast, a significant decrease in the crystallite size is observed in the [110] direction (along the CoO_2 layers), from about 34 nm (LC-1 min) to 12−15 nm (LC-5 h), and then it levels off until LC-7 d. From these results, two reaction paths could be at first glance considered to account for the β-$HCoO_2 \rightarrow LiCoO_2$ transformation: a dissolution/precipitation process or a H^+/Li^+ cationic exchange. Because no monotonous evolution in the cell parameters can be spotted along this transformation, we are here more likely dealing with a dissolution process, consistent with the drop in the crystallite size along the [110] direction, giving a clue as to the formation of smaller $LiCoO_2$ domains compared to the initial phase. To confirm this dissolution/crystallization process, we performed high-resolution transmission electron microscopy/selected-area electron diffraction (HR-TEM/SAED) observations (Figures 3 and 4). First, β-$HCoO_2$ particles are precipitated as large hexagonal platelets (Figure 3a). When the reaction proceeds through aging of

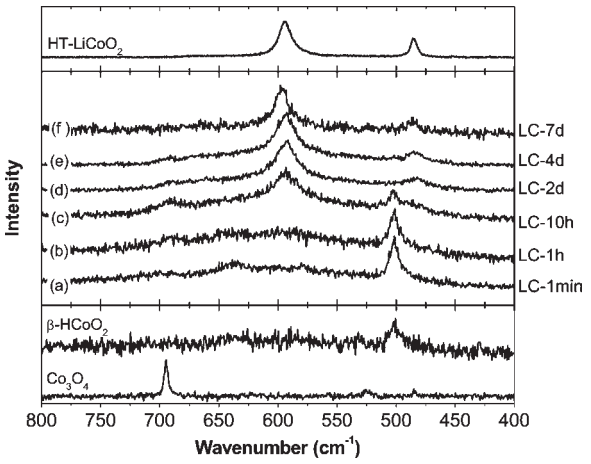

Figure 5. Raman spectra for LC-1 min, LC-1 h, LC-10 h, LC-2 d, LC-4 d, and LC-7 d. Raman spectra for HT-$LiCoO_2$ (top) and β-$HCoO_2$ and Co_3O_4 (bottom) are shown as reference.

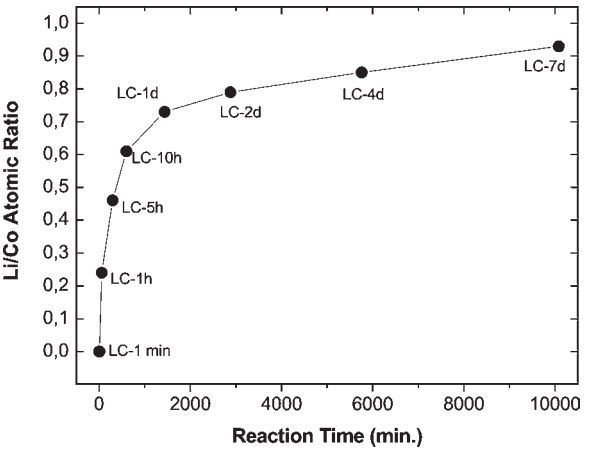

Figure 6. Evolution in the Li/Co atomic ratio in the precipitates as a function of the aging time at 60 °C of an ethanol solution initially containing $[Li^+] = 2\ mol \cdot L^{-1}$ and $[Co^{II+}] = 0.4\ mol \cdot L^{-1}$.

the suspension, the particle size undoubtedly decreases (Figure 3b,c). The SAED patterns clearly exhibit characteristic rings of polycrystalline samples. HR-TEM images of LC-1 min (β-$HCoO_2$) show a wave in the $HCoO_2$ layer stacking due to the presence of a large number of defects (Figure 4a). After 30 min, a progressive dissolution of this material is evidenced by the presence of numerous holes (Figure 4b). Beyond 5 h of reaction, $LiCoO_2$ crystals are formed with perfectly stacked Co−O layers without any corrugation (Figure 4c). Such an improvement in the crystalline order can only be explained by a two-step dissolution/precipitation process because a H^+/Li^+ cationic exchange would have most likely induced additional defects. The LC-7 d end-of-reaction sample (Figure 4d) only contains $LiCoO_2$ crystals, 4−13 nm in length.

While a simple H^+/Li^+ ion exchange from lamellar $HCoO_2$ would have most likely produced the lamellar HT-$LiCoO_2$ phase, this is not so trivial during a dissolution-based process. Even if the c/a ratio for the precipitated Li−Co−O phases is very close to 5, the size-induced expansion of the c parameter calls for another proof of the lamellar-ordered structure of the powders herein prepared. This can be achieved by Raman spectroscopy[24] because two signals are present for HT-$LiCoO_2$ (595 and 486 cm^{-1}) and four distinct bands are expected for LT-$LiCoO_2$ (603, 583, 478, and 445 cm^{-1}). In order to limit heat-induced evolution under beam exposure, we recorded Raman spectra with a low laser power (0.5 mW; Figure 5). The spectra for LC-1 min and LC-1 h confirm the precipitation of β-$HCoO_2$ with a main band at 501 cm^{-1}, in agreement with XRD and microscopy data. After 5 h of reaction, two bands located at 592 and 485 cm^{-1} and characteristic of HT-$LiCoO_2$ progressively grow at the expense of the lithium-free mother phase. Consistent with XRD and HR-TEM data, LC-10 h is a two-phase mixture. Finally, for longer reaction times (LC-2 d to LC-7 d), no further evolution can be noticed on the spectra typical of the HT phase. Aside from the peaks related to $HCoO_2$ and $LiCoO_2$, a small signal at around 700 cm^{-1} (from LC-10 h to LC-4 d) can be attributed to Co_3O_4. Surprisingly, in this study, this oxide has never been detected by XRD or HR-TEM, and, furthermore, the cobalt mos is very close to 3 (±0.03) all along the aging process. This rules out the presence of a significant amount of this low-oxidation-state phase but rather suggests a postdecomposition of $HCoO_2$ into Co_3O_4 under the Raman laser beam as previously observed.[25] The maximum Co_3O_4 content for LC-10 h is a consequence of two opposite evolutions: one is the progressive consumption of $HCoO_2$, and the other is a faster decomposition for smaller $HCoO_2$ domains produced throughout dissolution, and so for longer aging times.

Because we previously experienced some deviations from the expected stoichiometry (Li/Co = 1) for the directly precipitated powders in different alcohols, we also checked evolution in the Li/Co ratio for the aged samples at 60 °C (Figure 6). It turned out that the lithium content continuously increases, quickly at the early stage (Li/Co = 0.24 for LC-1 h) and then more slowly, to asymptotically reach a maximum value of 0.93 for LC-7 d. On the basis of our above characterization results, an incomplete reaction leading to the presence of residual $HCoO_2$ is not possible. We previously proposed[18] a very simple model accounting for the lithium deficiency in nanometric $LiCoO_2$ particles due to the presence of protons instead of lithium on the outer surface of the (00l) edge planes. A good fit with our observations was obtained through a simple model and a related relationship, $Li/Co = (n - 1)/n$, where n is the number of (00l) planes within the particles. In the present case, we can evaluate the n value for LC-7 d from 10 to 13 planes based on the crystallite size and direct HR-TEM observations, leading to a Li/Co value equal to 0.90−0.92, very close to that of the elemental analysis of this sample (0.93). Taking the Li/Co atomic ratio into consideration, LC-1 h (Li/Co = 0.24) should exhibit some HT-$LiCoO_2$ contribution in its XRD and Raman signals. Along that line, no change in these signals can be spotted from LC-1 d and LC-7 d, whereas their Li/Co atomic ratio evolves from 0.73 to 0.93. Such an observation suggests the existence of some solid solution domains for the end members of the binary system, waiting for further clues.

The impact of the solvent on the particle size of precipitated materials has been largely reported.[18,26−28] More specifically,

(24) Huang, W.; Frech, R. *Solid State Ionics* **1996**, *86−88*, 395.

(25) Pauporté, T.; Mendoza, L.; Cassir, M.; Bernard, M. C.; Chivot, J. *J. Electrochem. Soc.* **2005**, *152*, C49.

(26) Stöber, W.; Fink, A.; Bohn, E. *J. Colloid Interface Sci.* **1968**, *26*, 62.

(27) Hu, Z.; Oskam, G.; Searson, P. C. *J. Colloid Interface Sci.* **2003**, *2663*, 454.

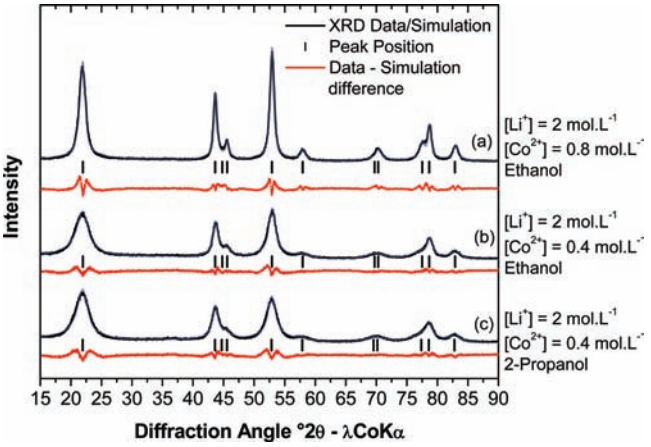

Figure 7. XRD patterns of nanometric $LiCoO_2$ obtained in (a) an ethanol solution with $[Li^+] = 2\ mol \cdot L^{-1}$ and $[Co^{II+}] = 0.8\ mol \cdot L^{-1}$, (b) an ethanol solution with $[Li^+] = 2\ mol \cdot L^{-1}$ and $[Co^{II+}] = 0.4\ mol \cdot L^{-1}$, and (c) a 2-propanol solution with $[Li^+] = 2\ mol \cdot L^{-1}$ and $[Co^{II+}] = 0.4\ mol \cdot L^{-1}$ after 7 days.

the length of the alcohol ($C_nH_{2n+1}OH$) carbon backbone impacts the dielectric constant that is involved in the precipitation mechanism. Namely, the longer the chain, the larger the crystallite/particle. As an explanation, a high dielectric constant favors the nucleation step, i.e., the formation of small crystallites, whereas a low dielectric constant favors the growth step, leading to large crystallites. Because we previously scrutinized this parameter for short reaction times,[18] we repeated several experiments while aging at 60 °C. With $[Li^+] = 2\ mol \cdot L^{-1}$ and $[Co^{II+}] = 0.4\ mol \cdot L^{-1}$, no effect of the alcohol chain length is observed on the crystallite size (Figure 7). Indeed, with ethanol (Figure 7b) and 2-propanol (Figure 7c), the crystallite sizes along [003] are 4.2 and 3.9 nm, respectively. This is consistent with the role that the alcohol nature mainly plays on the kinetics of the precipitation process, while the precipitation is thermodynamically controlled in the present case. When the supersaturation ratio[16] is increased by using higher $[Co^{II+}] = 0.8\ mol \cdot L^{-1}$, the growth step is favored and $LiCoO_2$ with a larger crystallites size (7 nm) can be precipitated (Figure 7a).

Whereas not the main aim of this paper, we tested the electrochemical Li-ion reactivity of all of the samples recovered along the aging. We have to keep in mind that the $LiCoO_2$ particles size was found during this aging and that these samples mainly differ in their $HCoO_2/LiCoO_2$ phase proportion. The charge capacities continuously increase from 29 (LC-1 min) to 158 $mAh \cdot g^{-1}$ (LC-7 d) (Figure 8a) with a reactivity mainly occurring between 3.7 and 4.2 V vs Li^+/Li^0. However, this charge capacity is not proportional to the initial lithium quantity because LC-1 d (Li/Co = 0.73) and LC-7 d (Li/Co = 0.93) have similar capacities (ca. 160 $mAh \cdot g^{-1}$). Thus, some parasitic reactions more likely occur on these highly divided phases as oxidation proceeds, and the first-cycle reversibility is very poor for all of the samples (e.g., 24% for LC-1 min and 42% for LC-7 d; Figure 8b). Unlike the charge capacities, the discharge capacities evolve linearly with the initial Li/Co atomic ratio (inset in Figure 8b), showing that the "H^+" amount does not influence the capacity of the electroactive phase, which is more likely

(28) Hu, M. Z.-C.; Payzant, E. A.; Byers, C. H. *J. Colloid Interface Sci.* **2000**, *222*, 20.

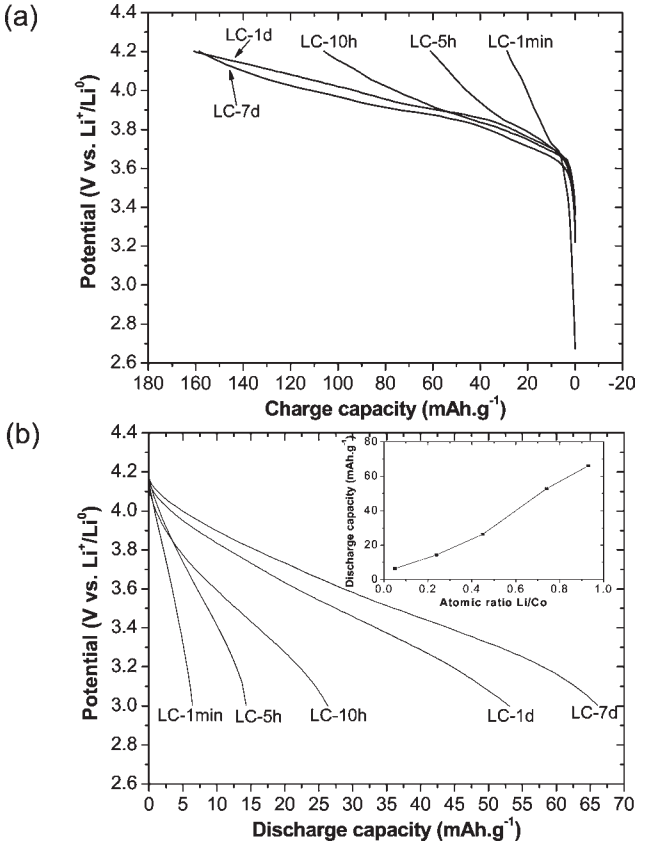

Figure 8. Voltage−composition galvanostatic curves for (a) first charge and (b) first discharge (1 Li for every 10 h, 20 °C, 20% carbon) vs Li^+/Li^0 for LC-1 min, LC-5 h, LC-10 h, LC-1 d, and LC-7 d. Inset: Discharge capacity as a function of the initial Li/Co atomic ratio in the powder.

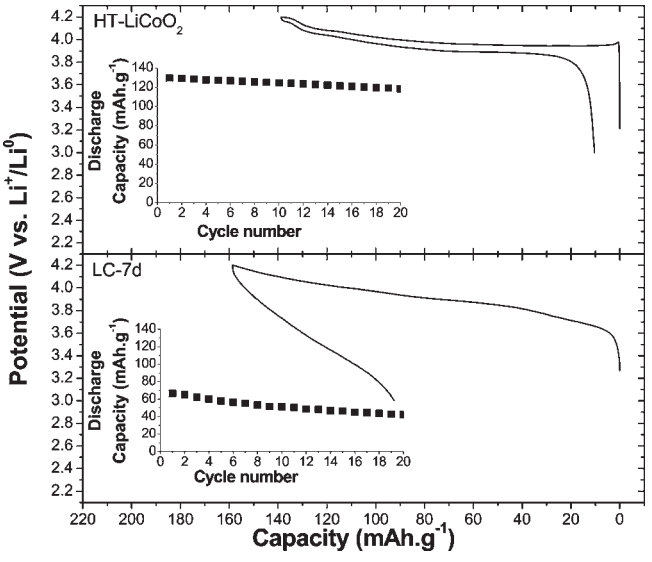

Figure 9. Voltage−composition galvanostatic curves (1 Li for every 10 h, 20 °C, 20% carbon) vs Li^+/Li^0 and the discharge capacity retention (inset) for bulk HT-$LiCoO_2$ (top) and LC-7 d (bottom).

governed by the amount of $LiCoO_2$ in the phase mixture. As we previously showed, the electrochemical behavior is more controlled by the divided nature of the materials, or indirectly by the surface reactivity through parasitic reactions, hence low-capacity retention. For instance, LC-7 d presents much lower capacity retention (63% after 20 cycles) than bulk

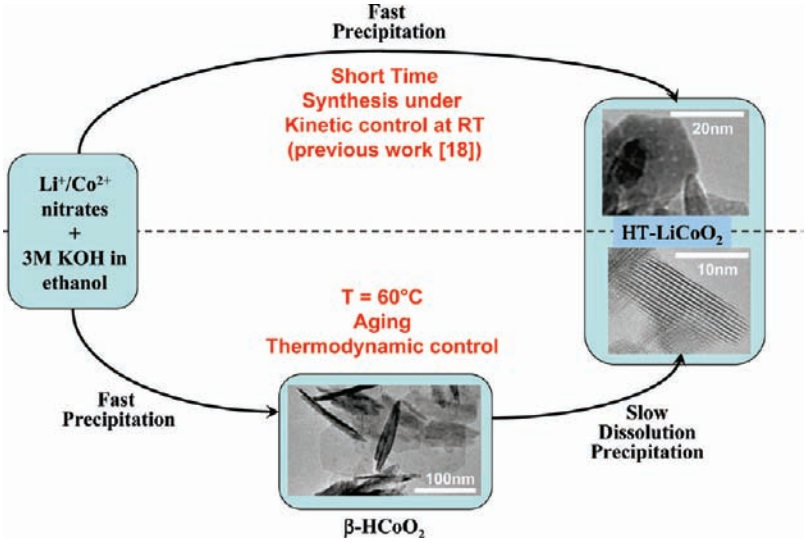

Figure 10. Reaction mechanism for the synthesis route described in the present work using an aging process in alcoholic media compared with the precipitation process described in ref 18.

materials (95%) (Figure 9). Finally, we noticed a large polarization that we suspect to originate from "surface protons" and that could result in some limitations in the kinetics of the charge-transfer process. The capacity retention is, however, better for these materials compared to the nonaged samples.[18] In view of future applications, further studies are now underway to modify the surface and to prepare proton-free small-sized samples.

Conclusions

We demonstrated in this paper the possibility of forming nanometric lamellar HT-$LiCoO_2$ powders in an alcoholic medium with increased Li/Co ratios compared to our previous work.[18] The two routes are summarized in Figure 10. In the present work, after the initial fast precipitation of the β-$HCoO_2$ phase in alkaline ethanol solutions, dissolution/recrystallization takes place, leading to well-crystallized HT-$LiCoO_2$ nanoparticles of about 4 nm $\times$ 13 nm in size. Some residual surface protons have been evidenced and presumably localized on the outer (00*l*) planes. The use of such an aging process allows to avoid the presence of Co_3O_4 and $Li_xCo_{1-x}O$ impurities, in contrast to direct precipitation methods in alcoholic media, as previously studied.

However, the still poor electrochemical performances of these nanometric $LiCoO_2$ powders are nested in the presence of surface protons together with the enhanced parasitic reactions related to their highly divided state. This calls for further investigations aimed at controlling the surface reactivity through either controlled thermal treatment or interface modification by coating. This will be addressed in a forthcoming paper.

Acknowledgment. The European Space Agency is acknowledged for its financial support.